

ScienceDirect



IFAC PapersOnLine 55-27 (2022) 62-67

The effect of the blade number on a cross-flow hydrokinetic turbine

Xian Wu*, Hsing-nan Wu**, Lei Zuo*, Bang-fuh Chen**

*Mechanical Engineering Department, Virginia Tech, Blacksburg, VA, 24061, USA (e-mail: leizuo@vt.edu)

**National Sun Yat-sen University, 70, Lian-hai Rd, Gushan District, Kaohsiung City, Taiwan (e-mail: d085040003@g-mail.nsysu.edu.tw)

Abstract: The effect of the blade number of a cross-flow hydrokinetic turbine is studied in this paper. To begin with, a blade cross-sectional shape NACA0025 is selected, as was used in a previous study. Secondly, after the turbine blade is modeled, the simulation cases are conducted numerically by use of a commercial package program, ANSYS Fluent. Before further analysis is conducted, validation is executed to make sure the calculation is reliable. The result shows that the blade number has effect on the turbine's efficiency or power coefficient (Cp). A 2-bladed, 3-bladed and 4-bladed turbine can obtain Cp values of 37.5%, 33.6% and 30.2%, respectively. Additionally, from the component torque yields gained by upper and lower surface of a blade respectively, it is revealed that the lower surface obtains much more torques than upper surface does during rotational range from 20° to 180°. Also, during this rotational range, the 2-bladed turbine proved to be more efficient than the other two cases. In contrast, the upper surface gained more torque yields than lower surface during rotational interval from 180° to 380°(=20°). And during this rotational interval, the torque yields obtained by the upper surface offset the lower surface torque yields, which made the total torque yields seem insignificant. The reduction of the blade number is thought to be the cause of efficiency enhancement due to less complex flow condition caused by the interaction of the blades upon rotation.

Copyright © 2022 The Authors. This is an open access article under the CC BY-NC-ND license (https://creativecommons.org/licenses/by-nc-nd/4.0/)

Keywords: CFD, cross-flow hydrokinetic turbine, renewable energy

1. INTRODUCTION

Due to the excessive use of fossil fuel and its impact on global warming, renewable energies have drawn more and more attention in recent years and broken down into several diverse kinds. Hydrokinetic turbines are generally classified as axial-flow type and cross-flow type. The former is also referred to as the horizontal-axis water turbine, and the latter is also known as a vertical-axis water turbine (VAWT). In this paper, the output power performance of cross-flow hydrokinetic turbine (CFHT) is discussed due to its advantage of directional insensitivity to the current flow. Fig. 1 is a demonstrative sketch that shows a variety of CFHT developed by Blue Energy Company.

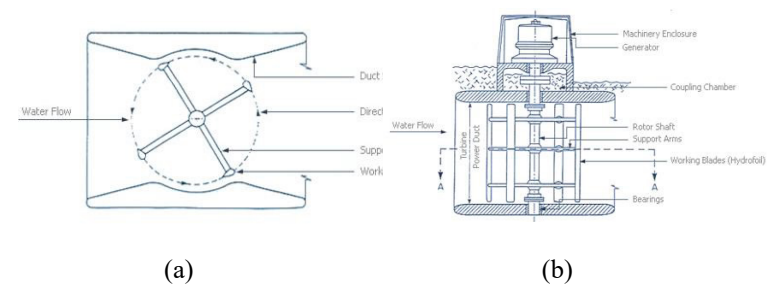


Figure 1 (a) Top view, (b) side view of the Blue Energy Hydro Turbine (Source of figure: http://www.bluenergy.com/vertical-axis-turbine/vaht/)

Being similar to the idea of wind turbine development, the concept of hydrokinetic turbine development is mainly originated from the wind turbine design. In the 1970s, analytical solutions were brought up to predict the performance of a cross-flow hydrokinetic turbine (Wilson and Lissaman, 1974; Strickland, 1975). Soon afterwards, Shankar (1979) made some revisions to these aforementioned studies [3]. More recently, Paraschivoiu (2001) compiled some analytical solutions and published a treatise on the development of a Darrieus-type turbine.

Nonetheless, the flow conditions may be complicated on account of turbulence or the domain geometry. These complications make it difficult for analytical solutions to predict the torque and power of the vertical turbine. CFD method is thus widely considered to be capable of evaluating the performance of the cross-flow (vertical-axis) turbine. Difficult predictability with respect to hydrodynamic characteristics can be boiled down to the complex flow conditions especially upon the rotation of the turbine. This is believed to be the main cause that influences the turbine output torque significantly. To facilitate this numerical calculation, the Moving Mesh technique (sliding mesh in particular) is comprehensively employed to conduct the research pertaining to CFHTs (or VAWTs) (Rao et al., 2020; Ashwindran et al., 2019; Mejia et al., 2021). Fluid dynamic phenomena of a cross-flow hydrokinetic turbine using moving mesh method incorporated with the turbulent model are investigated (Rao et al., 2020; Ashwindran et al., 2019). Islam et al. (2008) investigated hydrodynamic characteristics such as flow conditions, the lift coefficient, drag coefficient, force coefficient are evaluated by CFD method to compare with the experimental data.

While the aforesaid relevant works are conducted to investigate the aerodynamic or hydrodynamic characteristics, the improvement of a CFHT's performance is also discussed by other researchers. The performance improvement analysis falls into several categories, such as pitch control or duct

installation. The influence of pitch angle on the performance of a CFHT is simulated in Chen and Kuo (2013), with the result being reported that the power coefficient is the highest at the pitch angle of 5°. In the research work done by Hwang et al. (2009), controllable pitch angles were employed to maximize the CFHT's performance at various operating conditions. The optimized result shows an improvement in performance of around 25%.

To enhance the CFHT's performance, channeling devices are installed surrounding or on the sides of the turbine (Kirke, 2005; Ponta and Dutt, 2000). In these two previous findings, Kirke (2005) adopted ducted devices together with pitch control to increase the turbine's performance by two times. Ponta and Dutt (2000) used channeling devices and indicated that at low current speeds the channeled turbine outperformed the bare turbine without any ducts installed, although the ducted turbine's performance is poorer at faster current speeds than that of a bare one.

Unlike the aforestated idea that described the augmented flow velocity's effect of channeling devices on the increase of the turbine's performance or the change of pitch angles on the output power rise, this paper is aimed to investigate the performance of a CFHT by sheer use of blade number, instead of installing a duct or a channeling device. That is, the implementation and maintenance costs of shroud and duct installation are higher; the fatigue caused by incessant movement of the changing pitch of the blade can be unpredictable. With this idea in mind, three different numbers, namely two, three and four, are discussed in section three to study the turbine's efficiency before numerical methods are explained in section two. Moreover, discussions in section three are elucidated with the help of the illustration explanations of pressure distribution contours and velocity vector fields. After comparative discussions, the paper ends with some brief conclusions.

2. NUMERICAL METHOD

2.1 Hydrodynamic characteristics of the vertical-axis water turbine

Hydrodynamic characteristics of a cross-flow hydrokinetic turbine are stated in plenty of research publications, one example of which is found in Shiono et al. (2000). In this section, the hydrodynamic characteristics of a CFHT are briefly explained.

As shown in Fig. 2, the free stream water current flows at the velocity V_{∞} and V_a are the incoming velocity before the water flows into the turbine. Suppose the turbine rotates at the speed of ω . W is the relative velocity at the certain angle θ . V_c and V_n are the velocity components of W and are expressed as

 $\begin{aligned} &V_c = R\omega + V_a \cos\theta \\ &V_n = V_a \sin\theta \\ &W = [(V_c)^2 + (V_n)^2]^{1/2} \end{aligned}$

The included angle between W and the blade chord is called the angle of attack, which is defined as $\alpha = \tan^{-1}(V_n/V_c)$.

In Fig. 2, the water current acting on the blade will induce the lift force as well as the drag force, which are denoted by F_L and F_D, with their lift coefficient and drag coefficient C_L and C_D. F_L has both normal and tangential components, and so does F_D. The normal and tangential forces of F_L and F_D are denoted as F_N and F_T, with their corresponding force coefficients C_N and C_T defined by

 $C_T = C_L \cos \alpha - C_D \sin \alpha$

 $C_N = C_L \cos \alpha + C_D \sin \alpha$

Thus the normal force and tangential force can be obtained from

$$F_T = C_T(0.5\rho)CHW^2$$

 $F_N = C_N(0.5\rho)CHW^2$

where ρ is the fluid density, C is the blade chord and H is the height of the turbine.

From the above equation, the tangential force F_T , which moves the turbine blade, is the function of W, and W is the function of θ . Consequently, F_T can be written as $F_T(\theta)$. The average tangential force on one blade can be calculated by the following expression.

$$F_{Tavg} = \frac{1}{2\pi} \int_0^{2\pi} F_T(\theta) d\theta \tag{1}$$

Accordingly, the total generated torque (Qtotal) and mechanical output power (Pout) are

 $\begin{aligned} &Q_{total} = NF_{Tavg} R \\ &P_{out} = Q_{total} \ \omega \\ &\text{where N is the number of the blades, R is the radius of the} \end{aligned}$ turbine, and ω is the rotational speed.

In later sections, dimensional parameters together with non-dimensional parameters are both shown in illustrations at times. Torque coefficient is expressed as C_Q=Q_{total} $/(0.5\rho AV^2R)$ and power coefficient is expressed as $C_p = P_{out}/(0.5\rho AV^3)$. Additionally, regarding the torque gained by upper surface and lower surface of a blade, the upper surface C_Q and lower surface C_Q are defined as $Q_{up}/(0.5\rho AV^2R^*B^*2)$ and $Q_{down}/(0.5\rho AV^2R^*B^*2)$, respectively, where B is the blade number.

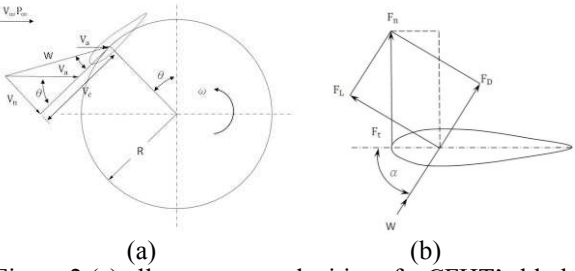


Figure 2 (a) all componet velocities of a CFHT's blade upon rotation. Free stream velocity is V_{∞} ; (b) Forces imposed on a blade

2.2 Governing equations

The turbine output torque is related to the change of the azimuthal angle. When the turbine starts to rotate, the complex turbulent flows make it difficult to solve F_T analytically. In some literature, although analytical solutions are derived, with the assistance of site experimental data to help predict the turbine's output performance, complex flow condition may yet pose an uncertain problem for analytical or semi-analytical solutions to be less accurate. Thus, CFD is adopted to obtain F_T at different rotational angle. The velocity field which influences F_T is dominated by the following governing equations in tensor form, i.e., continuity equation expressed in (2) and momentum equation incorporated with turbulence model expressed in (3).

$$\frac{\partial \rho}{\partial t} + \frac{\partial \rho \overline{u_j}}{x_j} = 0 \tag{2}$$

, where u_j is the mean flow velocity along x_j direction.

$$\frac{\partial \rho}{\partial t} + \rho \overline{u_j} \frac{\partial}{\partial x_j} (\overline{u_i}) = -\frac{\partial \overline{p}}{\partial x_i} + \rho g_i + \frac{\partial}{\partial x_j} (\mu \frac{\partial \overline{u_i}}{\partial x_j}) + \frac{\partial R_{ij}}{\partial x_j}$$
(3)

, where ρ is the fluid density, μ is viscosity, \bar{u}_j is the mean mean flow velocity along along x_i direction. \bar{p} is the mean pressure, and Rij is known as Reynolds Stress, expressed as

 $R_{ij} = -\rho u_i u_j$. (3) is also known as the Reynolds-averaged Navier-Stokes equations (RANS).

A package code, ANSYS 2019, which includes Fluent, developed by Finite Volume Method (FVM), used in current work, are adapted from (2) and (3) to solve the turbulence model. Moreover, k-ɛ realizable model is adopted in calculation of the turbulence model. SIMPLE algorithm and QUICK scheme are set for better accuracy.

The computational domain and boundary conditions in present study are illustrated in Fig. 4. The left side of the domain is set as the velocity inlet, right side as the pressure outlet. The upper and lower sides are set as symmetry to avoid blockage effect. The turbine blades are encased in a rotating area, where the outer and inner rings are set as interfacial boundaries. Some parts of the domain are densified particularly near the blade walls for better computational accuracy. The diameter of the rotating area is set to be D. The length and width of the domain are 20D and 12D. Other particulars of the operational settings, such as inflow velocity and hydrofoils, are also mentioned in section 2.3. Additionally, the mesh number used in present study is tested to range from around 38000 to 44000 by means of grid independence test.

2.3 Validation

Before the case studies in the next section, the numerical method is validated by three sets of experimental data. One is validated by the hydro turbine's starting torque obtained in Shiono et al. (2000), and another one is compared with the power coefficient shown in (Dai and Lam, 2009; Lain and Osorio, 2010). Fig. 3 is the designative drawing of the experiment rig used in Shiono et al. (2000), whose rotational radius R and height H of the tested turbine are 0.15 and 0.2m. Fig. 4 is the computational domain in reference to (Dai and Lam, 2009). The grid distribution layout is densified in certain region to pursue better computational accuracy.

Firstly, the results from Shiono et al. (2000) is used to validate our present work. The following are the operational parameters: water freestream velocity flowing at V=1.2 m/s with hydrofoil NACA63018. In addition, the solidity σ_1 is 0.366 (defined as NC/2 π R), where N is the blade number, R is the turbine radius and C represents the blade chord length. Tip speed ratio is expressed as $\lambda = \omega R/V$, where ω is the rotational speed.

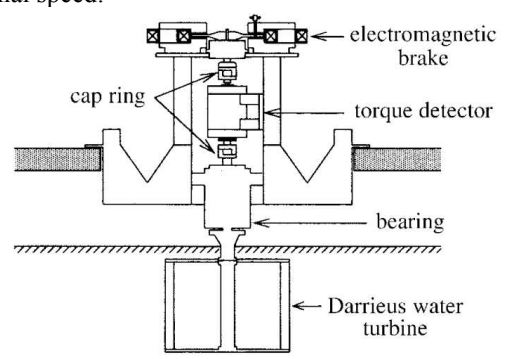


Figure 3 Turbine experimental test device. Source of figure: Shiono et al. (2000)

Fig. 5 is the comparison between present work and Shiono et al. (2000). From the figure, the maximal and minimal value difference (known as the amplitude) is more obvious for Shiono et al.. For present work, the amplitude is less remarkable. Despite some extrema seen in previous work of Shiono et al., the tendency between present study (presented in a continuous line connected with squares) and Shiono et al. (2000) (displayed in dashed line connected with triangles) is

shown to be similar, with the average difference of both studies being around 30%.

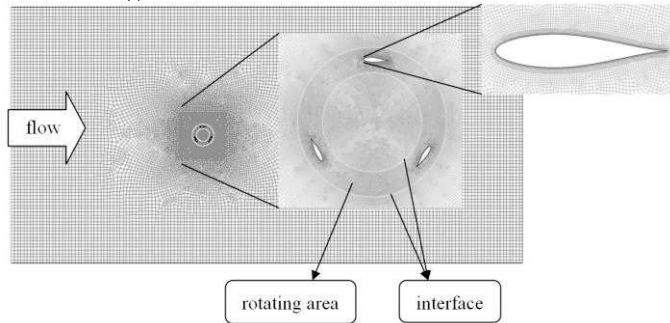


Figure 4 Computational domain and grid distribution

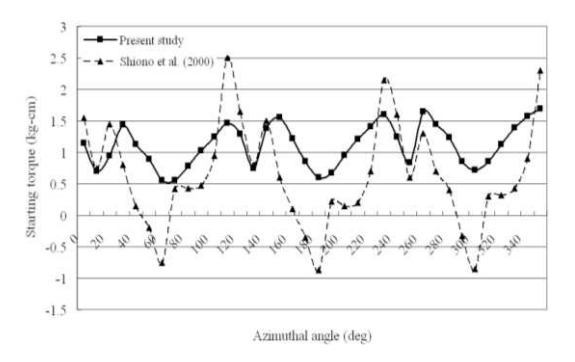


Figure 5 Comparison of starting torque at different azimuthal angle between present study and Shiono et al. (2000)

Another simulation comparison with Dai and Lam (2009) and Lain and Osorio (2010) are also carried out. The computational domain accompanied by grid layout is displayed in Fig. 4. Related parametric settings in this validation case are as follows: NACA0025 is adopted as the hydrofoil. Power coefficient is expressed as $C_p=P_{out}/(0.5\rho V^3S_{ref})$. P_{out} is the power yield. ρ is the water density and $S_{ref}=2RH$. Besides, $\lambda=1.745$ and $\sigma_2=0.89$ (defined as NC/R). More detailed parametric settings include: turbine height H=0.7m, R=0.45m, $\omega=3.87$ rad/s, $S_{ref}=0.63$ m², chord length=0.133m. Some zones in Fig. 6, such as blade walls, are magnified to exhibit the areas where the grids are densified in pursuit of computational accuracy. The region enclosed between two concentric circle interfaces is the moving zone with the passage of time.

Table 1. Cp comparison among three studies

	Present study	Dai and Lam (2009)	Lain and Osorio (2010)
Numerical	27.6	27.5	24.8
Others		21.5	26.5
		(DMS model)	(experiment)

Table 1 is the power coefficient comparison among three works, i.e. present study, Dai and Lam (2009) and Lain and Osorio (2010). Particularly, in the work of Lain and Osorio (2010), both simulation and experiment are carried out. Slight deviation (less than 2%) is found in all three numerical works (present study, Dai and Lam, Lain and Osorio), but when three numerical studies are compared with experimental data in Lain and Osorio (2010), more discrepancy is revealed. It is thought that the effect of 3D dimensionality brings about the deviation among all research results. With the exception of this deviation in Table 1,

overall agreement in like manner of turbine's performance is disclosed.

From what is shown above, the numerical result for the present work is slightly greater than the experimental data conducted by Shiono et al. (2000). The cause of the difference among any sets of the data can be ascribed to the transmission loss. Additionally, the difference can be partly due to the 2D model simulation failing to predict the real case accurately in 3D model simulation, in terms of the edge effect on top and bottom of the rotor. Furthermore, the comparison with Dai and Lam (2009) and Lain and Osorio (2010) is made. The result shows that a general tendency is observed. In summary, the general agreement between our present study and other works has built up our confidence in further investigations in later sections.

3. RESULTS AND DISCUSSION

Validations in the previous section have paved the way for more investigation for other operational parameters. In this section, a uniform stream flow is applied while turbines with three different blade numbers are studied to evaluate the effects on the performance of the VAWT. The blade numbers as an operational parameter are chosen as 2, 3, 4. Model profiles with mesh distribution of these three cases are illustrated in Fig. 6.

(a) (b) (c)

Figure 6 Model profiles with mesh distribution of three simulated cases. (a) 2 blades (b) 3 blades (c) 4 blades.

In the following passages, the model profiles of three cases are described first. Then, the overall turbine's performances are studied, followed by the output torque depiction of a single blade for each case. At certain specific azimuthal angles, pressure contours and plots are shown to interpret the physical characteristics with the different guiders to illustrate the advantage of the ameliorated models.

3.1 Case description

Fig. 7 is the descriptive sketch of the turbine as the top view. The turbine shown is a 3-bladed turbine, and the direction of freestream is shown by use of an arrow beside the sketch. The azimuthal angle or the rotational angle is included by the solid line and the dashed line, denoted as $\theta,$ and is determined based on the vertical line (y-axis). The solid line represents the initial time of simulation. The dashed line together with the dashed turbine represent the turbine's location after rotating to the angle of $\theta.$

In all three cases, the blade of the turbine is the same as the operational parameters of the NACA0025, which has been depicted in Section 2, with height and radius of the turbine selected to be 1m and 0.45m, respectively. In addition, the blade chord length is 0.133m, and the incoming flow velocity is set to be 1 m/s.

Given a uniform flow condition, the torque output curve is known to be periodic as far as a cross-flow turbine is concerned. Through the observation of the output torque curve, the influence of operational factors on the overall turbine output performance can be revealed. Firstly, the comparison of power coefficients among the three cases with (a) 2-bladed (b) 3-bladed (c) 4-bladed is displayed in Fig 8. From the figure, it is noticed that bell-shaped concave down curves in common tendency are exhibited amongst all three

cases. The maximal Cp values are 37.5%, 33.6% and 30.2% for the cases of 2-bladed, 3-bladed and 4-bladed configurations at the respective rotational speed of 5.5, 4.5 and 4 rad/s, which are shown using dotted circles of various colors. This means 2-bladed case can acquire the maximal power, while the least power yields are gained by the 4bladed case. If 4-bladed is chosen as the baseline, then 3bladed configuration reports a relative rise of 11.3% efficiency, and 2-bladed version can gain a relative increase rate of 24.2%. Moreover, the region near the best Cp is broader for 2-bladed than 3-bladed or 4-bladed. For 2-bladed, this region is observed to range from 4.5 to 6.5 rad/s; For 3bladed and 4-bladed, the region is 4 to 5.5 rad/s and 4 to 5 rad/s, respectively. This also represents that 2-bladed has a wider range to generate the best power output when compared to the other two cases.

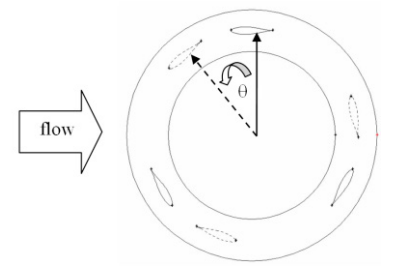


Figure 7 2D view of a three-bladed turbine on rotation at θ . 3.2 Comparison of power coefficient and torque yields

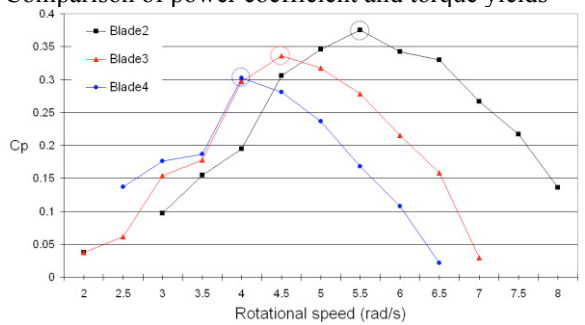


Figure 8 Turbine's power coefficient (Cp) of three simulated cases with respect to the change of rotational speed.

Thus, as previously mentioned concerning the three circles in Fig. 8, three simulation cases, namely 2-bladed at 5.5 rad/s, 3-bladed at 4.5 rad/s and 4-bladed at 4 rad/s, are chosen to demonstrate how the factor of blade number influences the turbine's performance. The corresponding data are shown in Fig. 9, which illustrates the torque yields period within a period. In Fig. 9, the upper and lower plots show the respective component torques obtained by the upper and lower surface of a blade respectively. The resultant torque is named as total, which stands for the sum of the torque gain by both the upper and the lower surface. It is revealed that the upper and lower surface torque yields together with the resultant torque over a period demonstrate an overall resembling trend except for some discrepancy of working range in Fig. 9(a), (b) and (c).

Nonetheless, concerning the upper and lower surface torque gain, each has an individual working range. Observed from all three simulation cases in Fig. 9, the lower surface torque output of all three figures becomes dominant and active at the angle around 20° to 180°, while the upper surface torque output in this interval becomes more dormant. Yet, from the angle past 180° to 380° (namely 20°), which is mainly the 3rd and the 4th quadrant of the rotating plane

shown in Fig. 7, the upper surface torque becomes more significant than the lower surface torque. It is also indicated that during the range from 180° to 360°, once a blade rotates near the angle of 90°, it serves to block the water current from flowing into the turbine's rotational range. This phenomenon, which can be seen from Fig. 10(d)-(f), accounts for the cause of the interaction among blades.

When the torque output plots of three respective cases in Fig. 9 are taken as guide, it is learned that the upper and lower surface of the blade has its individual working range. If one wants to enhance the torque output, one can resort to some areas where lower torque yields are reported. Take 2bladed case for example. The lower surface of the blade acquires more torque than the upper surface at rotational angle from 20° to 180°. The cause of this phenomenon may be due to the interaction of turbine blades. Please refer to Fig. 10(d)-(f) for the velocity contour. It is found that during the rotational interval from angle 120° to 200°, the current flow is influenced by the forefront blade. In this example where the blade is positioned at 100°, some current flow is blocked or interfered downstream due to the forefront blade moved to 100°. However, this also means the torque gain by the lower surface away from this interval can be enhanced by other devices or other method like pitch control. Such is the case with the upper surface. In all, if the torque output curve during some rotational interval is reported to be lower, then one can consider enhancing the torque within this rotational interval.

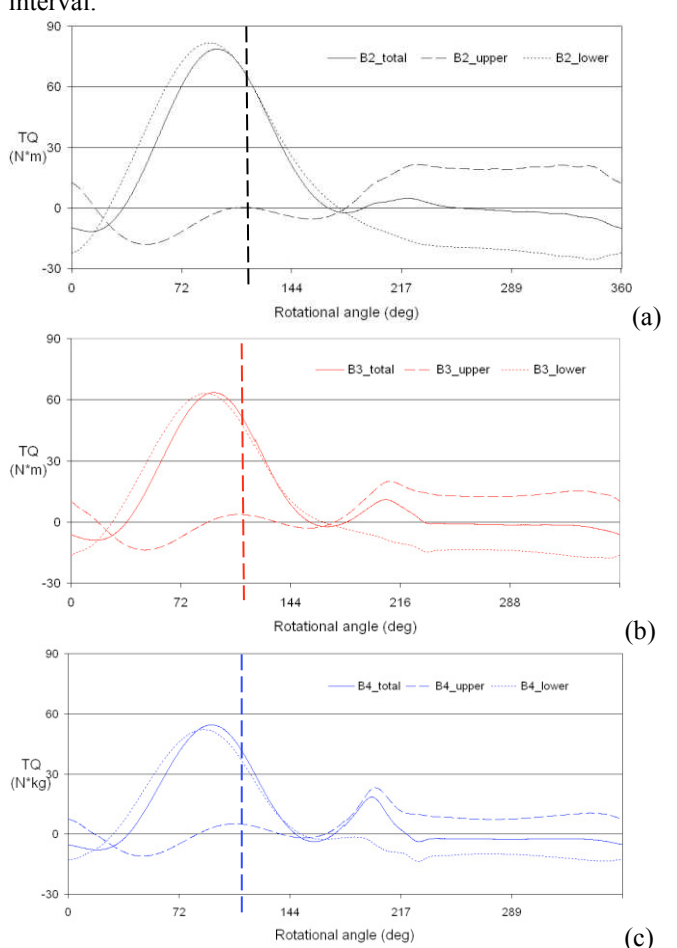


Figure 9 Torque yields over a rotational period of a blade.

(a) 2-bladed case (named B2) at 5.5 rad/s, average torques of total, upper and lower are 14.46, 6.07 and 8.39 (N*m). (b) 3-bladed case (named B3) at 4.5 rad/s, average torques of total, upper and lower are 11.0, 5.49 and 5.52 (N*m); (c) 4-bladed case (named B4) at 4 rad/s average torques of total, upper and lower are 8.57, 4.56 and 4.01 (N*m)

Through the observation of the average torque data in Fig. 9, it is understood that the torque yields acquired by lower surface are especially significant for the 2-bladed case. Regarding the 3-bladed case, the average torque gained by upper and lower surface of the blade is approximately equivalent. As for the 4-bladed case, the average torque gained by the upper case seems to dominate the total torque.

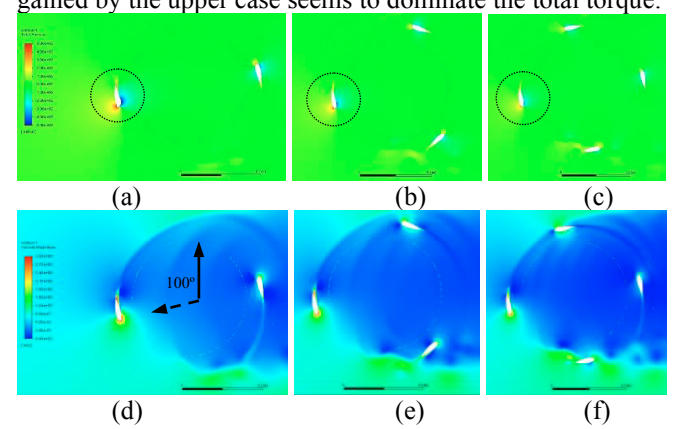


Figure 10 (a)-(c) Pressure contours, (d)-(f) velocity contours of three different cases at rotational angle 100°; (a)/(d) 2-bladed case at 5.5 rad/s, (b)/(e) 3-bladed case at 4.5 rad/s and (c)/(f) 4-bladed case at 4 rad/s.

Take rotational angle of 100° as an instance, which are the long vertical dashed lines of three respective simulation cases in Fig. 9, with the corresponding pressure and velocity contours in Fig. 10. From the 2-bladed case, namely Fig. 10(a), one may notice that the pressure acting on the lower surface varies more greatly from the leading edge to the trailing edge. This is ascribed to the velocity field caused by the current flowing around the blade at 100°, shown in Fig. 10(d). Since the pressure difference is greater, the forward force is then greater. Hence the subsequent torque is greater in Fig. 9(a). Comparatively, the other two examples of 3bladed case at the same angle 100° (long red vertical dashed line) in Fig. 9(b) and 4-bladed case also at the same angle 100° (long blue vertical dashed line) in Fig. 9(c), together with the corresponding pressure contour, are displayed in Fig. 10(b) and (c). It is known that the pressure difference on the lower surface is not as significant as mentioned in 2-bladed case. As a consequence, the subsequent torques of both 3bladed case and 4-bladed case at 100° [see the long vertical dotted lines shown in Fig. 9(b) and (c)] are then less significant than 2-bladed turbine.

Similarly, a general tendency of the resultant (total), the upper and the lower surface torque yields over a period is revealed in Fig. 9(a), (b) and (c). Related explanations at other rotational angles are similar to the example of 100° stated in the foregoing passages and are not elaborated in here for brevity. By way of the hydrodynamic characteristic analysis described formerly, a turbine's performance can be enhanced via ducted devices, pitch control or other related methods for future works.

4. CONCLUSION

After the explanation of numerical methods and validation process, confidence in computational simulation is built for further parametric investigation. Additionally, from what has been discussed in previous passages, some conclusions have been made:

Firstly, among all three simulation cases, the maximal Cp equivalent to 37.5% can be attained by the 2-bladed case, with its best output power region also the widest, about 4.5 to 6.5 rad/s. The performance of the 3-bladed case is second to the 2-bladed case with the maximal Cp equal to 33.6%, and the best power output region from 4 to 5.5 rad/s. For the 4-bladed case, however, the maximal Cp is 30.2%; its best power output region falls from 4 to 5 rad/s.

Secondly, the overall performance of a 2-bladed turbine mentioned above outshines the other two cases due to less interference of blade interaction. That being said, other turbine design factors, such as turbine balance or stress analysis are not taken into account so far. As a result, if other design factors are considered, the best performance of a CFHT may be not the 2-bladed turbine, but a 3-bladed one as is often adopted in practical engineering applications.

Lastly, the torque output plot with respect to the total, upper or lower surface are illustrated, and the dataset indicates that the torque output is influenced by the other blades within some working range. This implies the complexity of the flow regime is liable to the increase of the blade number, and hence the turbine's performance is affected. Within the rotational range from 20° to 180°, the lower surface can garner more torque than the upper surface. and the torque output reaches its peak near 90°. At this instant, the pressure difference applied on the blade is the largest, thus causing the forward force to be the greatest. Contrarily, within the rotational range from 180° to 360°, the upper surface dominates the torque yields. However, the gap between upper and lower surface during this interval becomes narrower with the increase of blade number. The more turbulent flow regime due to the blade interaction accounts for this phenomenon. Through the analysis of working range of either surface of a blade, torque gain can be enhanced by means of ducted plates, pitch control or related methods or devices.

In present paper, only three blade number configurations are studied so far. Some parameters to enhance the turbine's performance, such as solidity (changing with chord length), pitch angle control and many more, will be considered as possible future works.

5. ACKNOWLEDGEMENT

This research is partially funded by the U.S. National Science Foundation (NSF) under the Award No. 2134146 and partially supported by Taiwan's Ministry of Science and Technology for the Thousand Mile Horse Grant under the Contract No. 110-2917-I-110-003. Their financial assistance is greatly appreciated.

REFERENCES

Ashwindran., S., Azizuddin, N, A. A., and Oumer, A. N. (2019). Computational fluid dynamic (CFD) of vertical-axis wind turbine: mesh and time-step

- sensitivity study, Journal of Mechanical Engineering and Sciences
- Chen, C.C., and Kuo, C.H., (2013). Effects of pitch angle and blade camber on flow characteristics and performance of small-size Darrieus VAWT. Journal of Visualization.
- Dai, Y. M., and Lam, W. H., (2009). Numerical study of straight-bladed Darrieus-type tidal turbine, Energy.
- Hwang, I.S., Lee, Y.H., Kim, S.J., (2009). Optimization of cycloidal water turbine and the performance improvement by individual blade control. Apply Energy.
- Islam, M., Ting, D. S. K., Fartaj A., (2008). Aerodynamic models for Darrieus-type straight bladed vertical axis wind turbines, Renewable and Sustainable Energy Review
- Kirke, B., (2005). Developments in ducted water current turbines. (http://www.cyberiad.net/library/pdf/bk_tidal_paper25 apr06.pdf)
- Lain, S., and Osorio, C., (2010). Simulation and evaluation of a straight-bladed Darrieus-type cross flow marine turbine, Journal of Scientific and Industrial Research.
- Mejia, O. D. L., Mejia, O. E., Escorcia, K. M., Suarez F., and Lain, S. (2021). Comparison of Sliding and Overset Mesh Techniques in the Simulation of a Vertical Axis Turbine for Hydrokinetic Applications, Processes.
- Paraschivoiu, I. (2001). Wind Turbine Design with emphasis on Darrieus concept. Canada: Ecole Polytechnique de Montreal.
- Ponta, F., and Dutt, G. S., (2000). An improved vertical-axis water-current turbine incorporating a channelling device, Renewable Energy.
- Shankar, P. N. (1979). Development of vertical axis wind turbines.
- Shiono, M., Suzuki K., and Kiho, S., (2000). An experimental study of the characteristics of a Darrieus turbine for tidal power generation, Electrical Engineering in Japan.
- Strickland, J. H. (1975). The Darrieus turbine: a performance prediction model using multiple streamtubes, Sandia National Laboratories.
- Rao, P. V., Arun, H. H. D. S. S., Pasha, M K., and Lokesh R. (2020). Aerodynamic analysis of vertical axis wind turbine using CFD, High Technology Letters.
- Wilson, R.E., and Lissaman, P.B.S. (1974). Applied aerodynamics of wind power machines, National Science Foundation Report.